



Variability and combination as ensemble of mineral dust forecast during the 2021 CADDIWA experiment

Laurent MENUT¹

¹Laboratoire de Météorologie Dynamique (LMD), Ecole Polytechnique, IPSL Research University, Ecole Normale Supérieure, Université Paris-Saclay, Sorbonne Universités, UPMC Université Paris 06, CNRS, Route de Saclay, 91128 Palaiseau, France

Correspondence: Laurent Menut, laurent.menut@lmd.ipsl.fr

Abstract. As an operational support to the CADDIWA field campaign, the coupled regional model WRF-CHIMERE is deployed in forecast mode during the summer 2021. The simulation domain covers West Africa and the East Atlantic and allows the modeling of dust emissions and their transport to the Atlantic. On this route, we find Cape Verde which was used as a base for measurements during the CADDIWA campaign. The forecast consists of meteorological variables and mineral dust concentrations on a horizontal grid with a resolution of 30 km and from the surface to 200 hPa. Each day, the simulation starts the day before (D-1) and up to four days ahead (D+4). For each day, we thus have six different calculations, with logically a better precision the closer we get to the analysis (D-1). In this study, a quantification of the forecast variability of wind, temperature, precipitations and mineral dust concentrations according to the modelled lead is presented. It has been shown that the forecast quality doesn't decrease with time and that high variability on some days for some variables (wind, temperature) does not explain the behavior of other dependent and downwind variables (mineral dust concentrations). A new hypothesis is also tested: why not consider the several six forecast leads available for each date as members of an ensemble forecast? It has been shown that this new forecast, the mean of all forecast leads, is able to give better results for two AERONET stations on the four available for Aerosol Optical Depth. This could open the door to further testing with more complex operational systems.

1 Introduction

Over the western Africa, and during the boreal summer, mesoscale convective systems are moving from East to West and interact with easterly waves and mineral dust plumes, (Knippertz and Todd, 2010; Marsham et al., 2011). Leading the African continent to arrive above the Atlantic sea, they can generate tropical storms. This phenomenon is maximum during the month of September when the sea surface temperature is at its annual maximum. The magnitude of interactions between these systems and the mineral dust concentrations via the direct and indirect effects of aerosols on meteorology remain unclear, (Lavaysse et al., 2011). This motivated the deployment of the Clouds-Atmospheric Dynamics-Dust Interactions in West Africa (CADDIWA) field campaign, (Flamant et al., 2022). The measurements include long-term surface stations and dedicated airborne measurements. Aircrafts were located at Sal (Capo Verde), under the wind flow coming from western Africa. In addition to the local study of storms generation, these aircraft measurements were also thought to help the validation of space-borne products as those of Aeolus, EarthCare and IASI satellites missions, (Martin et al., 2021). In addition to these measurements,



25 numerical modelling is planned throughout the project. Simulations are organized following two different configurations: (i)
in forecast mode during the campaign, (ii) in analysis mode after the campaign. In the framework of this study, we present the
first configuration with the daily forecast made during the CADDIWA experiment.

Before to study the interaction between aerosols, clouds and radiation, it is important to qualify the accuracy of the used
models. Forecast is a useful tool for this kind of evaluation. The fact to simulate the same day several times with a different
30 meteorology is a way to quantify the model variability. It is close to an ensemble simulation, even if the number of members
is lower, (Atger, 1999; Toth et al., 2001; Richardson, 2001). Each day, six days are modelled including five in advance. By
comparing the several forecast simulations but for the same date enables to quantify the variability of the model.

Another aspect will be analyze in this study: as several forecast leads correspond to the simulation of the same period but with
different initial conditions for the meteorology, we can imagine that the leads are equivalent to ensemble modeling members.
35 Ensemble modelling is widely used in forecast of meteorology or air quality, (Delle Monache et al., 2006), (Vautard, 2006),
(Benedetti et al., 2018). But in general, the ensemble is built using the same model with perturbations. Some other techniques
exist such as the "poor man's ensemble" and are widely used in meteorology, (Ebert, 2001), (Buizza et al., 2003), (Bowler
et al., 2008). To our knowledge, these approaches are not used for Chemistry-transport Modelling (CTM). They consist in
using different models but making the forecast of the same period. Also in meteorology, they can be used in operational centers
40 to update the covariance matrixes used for the data assimilation.

In this study, we propose a complementary approach following the question: *Is it possible to use several forecast leads as if
it was an ensemble and improve the quality of the forecast?* If the result is positive, it means it is possible to run less ensemble
simulations each day, then a faster forecast, while still improving the quality of the forecast. And for those institutes that don't
have the computer resources to do ensemble simulations, it still allows them to have a probabilistic approach on their forecast.

45 The main goal of this study is thus first to quantify the variability on temperature, wind, precipitation rates, Aerosol Optical
Depth (AOD) and surface concentration of mineral dust as a function of the forecast lead. Second to try to establish some
correlations between possible differences. With this quantification, we can assess the robustness of the forecast and the degree
of confidence available for experimenters during such kind of field campaign. Section 2 presents the modelling system and
the studied period. Section 3 presents the results of the comparison between the several forecast leads. Section 4 presents a
50 tentative approach of mixing several leads for the same day in order to mimic an ensemble forecast. Results are compared to
AERONET Aerosol Optical Depth measurements. Section 5 presents conclusions of the study.

2 The modeling system

2.1 The modelling tools

In this study, we use the WRF-CHIMERE model built with WRF 3.7.1, (Powers et al., 2017), and CHIMERE 2020r3, (Menut
55 et al., 2021). These two models are coupled using the OASIS3-MCT external coupler, (Craig et al., 2017). The WRF model
is forced with the global scale forecast fields from NCEP Global Forecast System (GFS), (Halperin et al., 2020). For this
experiment, a specific configuration was designed, different from the analysis use, in order to have a lower numerical cost.



Indeed, the goal was to launch the simulation for six days, from (D-1), the day before the current date to (D+4) four days in advance. This long forecast was designed to permit to the aircraft scientific researchers to have enough time to decide what flight plan to use, depending on the meteorological situation to come. The simulation is launched at midnight to benefit from the last forecast meteorological field and much finish around 5 am, including all post-processed figures. These constraints of real-time forecast led to have a light version of the model where only mineral dust are modelled. The model is also used in offline mode, meaning that there is no retroaction of aerosols on meteorology, in order to ensure the stability of the calculation. Mineral dust are modelled with ten bins from 0.01 to 40 μm . The dust emissions scheme used is the one of Alfaro and Gomes (2001), modified by Menut et al. (2005). Note that the CHIMERE model is also daily used in forecast mode for air quality with all available processes, being operated by operational centers, (Rouil et al., 2009; Marécal et al., 2015).

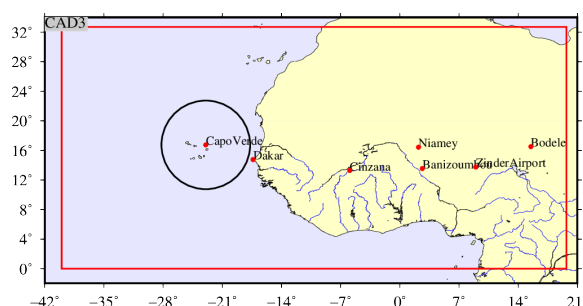


Figure 1. Model domain in red, with the main studied locations: from East to West: Bodélé, Zinder, Banizoumbou, Niamey, Cinzana, Dakar, Capo Verde. The black circle is the possible range of aircraft measurements during the campaign.

The model domain, **Figure 1**, is defined with the same horizontal grid for WRF and CHIMERE and covers a part of Atlantic sea and western Africa, from -40°E to $+20^{\circ}\text{E}$ in longitude and 0° to 33°N in latitude. It is constituted of 200×110 cells with a constant resolution of 30 km. The WRF model has 32 vertical levels from the surface to 50 hPa. CHIMERE has less vertical levels with 15 layers from the surface to 300 hPa. This domain was designed to be able to model at the same time: (i) mineral dust emissions in Africa, from Dakar to Bodélé, (ii) model transport from Africa to Atlantic sea, (iii) have the measurement site of Capo Verde not too close to the domain boundaries. In **Figure 1**, the locations of Capo Verde, Dakar, Bodélé, Zinder, Niamey, Banizoumbou, Cinzana are reported. Model results were daily extracted at these locations for the experimenters based in Capo Verde with the aircrafts. The circle indicates the possible range of aircraft measurements during the campaign.

2.2 The measurements

This study is mainly a model versus model study. The focus is not performed on comparison between model and measurements. It will be done only at the end of the study with a comparison of measured versus modeled Aerosol Optical Depth (AOD). The AEROSOL ROBOTIC NETWORK global remote sensing network (AERONET, <https://aeronet.gsfc.nasa.gov/>) level 1.5 measurements are used for this comparison, (Holben et al., 2001). The AOD at a wavelength of $\lambda=675$ nm are daily averaged and compared to daily averaged modelled values.



Station Name	Longitude (°E)	Latitude (°N)
Bodélé	15.5	16.5
Zinder	8.98	13.75
Banizoumbou	2.66	13.54
Niamey	2.2	16.43
Cinzana	-5.93	13.28
Dakar	-17.36	14.75
CapoVerde	-22.95	16.75

Table 1. List of the AERONET sites used for the comparisons between measured and modelled AOD.

2.3 The modelled period and the Intensive Observation Periods

The field campaign was carried out from 8 to 21 September 2021, with airborne measurements around Sal Island in Capo Verde, (Flamant et al., 2022). In order to have a tested and robust forecast modelling system, the daily forecast started 10 August 2021 and ended 1st November 2021. Among all observations periods, two events were observed: the tropical perturbation called Pierre-Henri, passing over Sal on 11 September and the period from 17 to 24 September with the passage over Sal of the two Tropical Cyclones, called Peter and Rose. In this study, the results will be presented over two periods:

- section 3: only from 1st to 30 September 2021 for the part about the variability of the forecast during the CADDIWA field experiment.
- section 4: over the whole modelled period, from 10 August 2021 to 1st November 2021, for the part about the merge of forecast leads.

For the results presentation, there is several possibilities. As presented in Figure 2, each day, the modelling system runs to simulate 6 days, from (D-1), the day before, to (D+4) four days in advance. With all these simulations, results may be discussed following two ways:

1. Comparison of all leads for one date: For example, for the 11 September at 16:00 UTC, we can display the result of the simulations performed:
 - 12 September, forecast hour -8, (D-1)
 - 11 September, forecast hour 16, (D+0)
 - 10 September, forecast hour 16+24=40, (D+1)
 - 9 September, forecast hour 40+24=64, (D+2)
 - 8 September, forecast hour 64+24=88, (D+3)

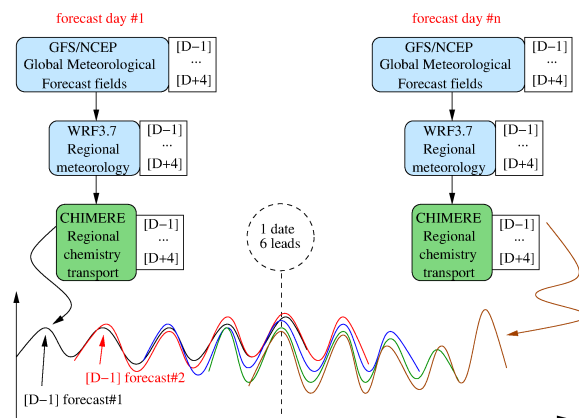


Figure 2. Principle of the modelling system in forecast mode. Each day, the global meteorological fields are downloaded to force the region WRF model. These regional fields are used to drive the CHIMERE chemistry-transport model, mainly for mineral dust emissions, transport and deposition. The procedure is repeated every day.

- 7 September, forecast hour $88+24=112$, (D+4)

This comparison may be achieved with maps and vertical cross-sections.

2. Comparison between leads during the whole period: It is possible to build time-series using the (D-1) for all days, the (D+0) for all days until (D+4) for all days. In this case, we can calculate statistical scores between the time-series as if they were different model realizations.

105

In the following sections and the Appendix, when analysis consists in maps or vertical cross-sections, we selected the 11 September 2021 to present the results, being the day when the "Pierre-Henri" tropical storm was diagnosed above Sal, in Capo Verde Island, (Flamant et al., 2022).

3 Variability of forecast leads during CADDIWA experiment

110 Results are presented as statistical scores (defined in Section 3.3). They are calculated for data over Bodélé and Capo Verde. The main goal being to compare the simulation leads and evaluate the variability from one lead to the next, there is no measurements in the analysis but only model versus model. The initialization of the model being performed using analyzed meteorological fields, (Halperin et al., 2020), the simulation of (D-1) is considered as the reference.

3.1 Time-series of surface mineral dust concentrations

115 Time-series are presented for two sites, Bodélé and Capo Verde. They are located on a Sahelian iso-latitude transect and often used to quantify the amount of mineral dust emitted in the Saharan desert and after long-range transport of these dust,

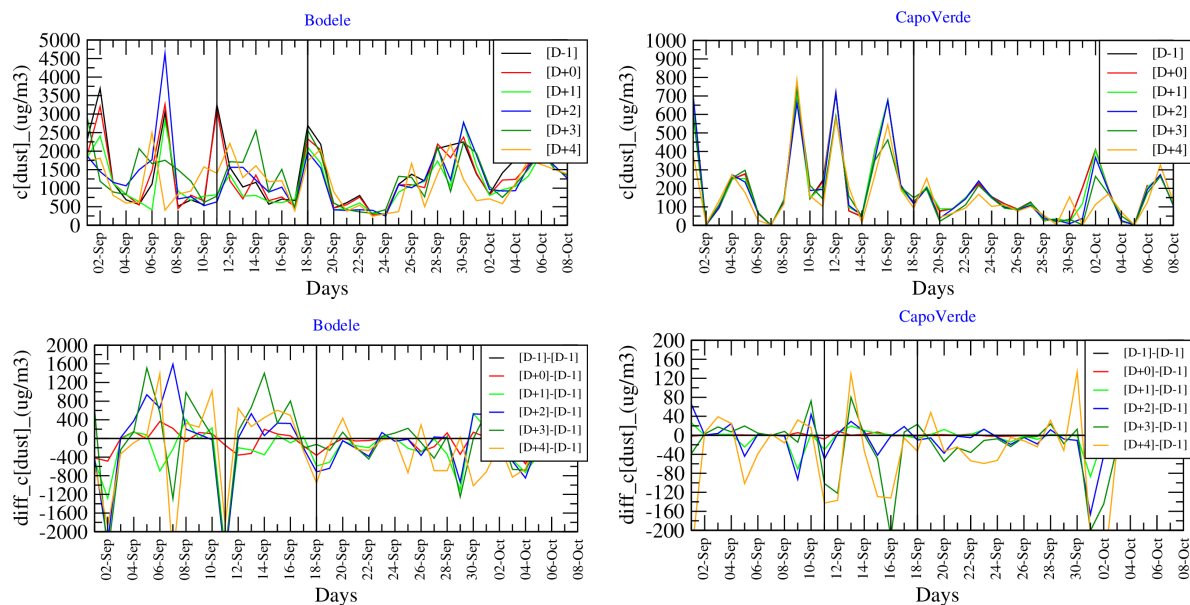


Figure 3. Time-series of surface mineral dust concentrations ($\mu\text{g}\cdot\text{m}^{-3}$) for each lead and of differences between leads.

respectively, (Marticorena et al., 2010). **Figure 3** presents time-series for the surface mineral dust concentrations ($\mu\text{g}\cdot\text{m}^{-3}$). The variability of the forecast for these concentrations should be the result of a mix between the variabilities calculated with the 10m wind speed (an important parameter for the sources) and the precipitation (a major sink). In Bodélél, the surface concentrations varies a lot between 0 and 5000 $\mu\text{g}\cdot\text{m}^{-3}$. It seems huge but it is classical when being just over the main Saharan source. The mass is composed of a large mass distribution and the major part of big particles are deposited before transport, close to the source. The variability from one lead to another is important and illustrates the impact of the wind speed variability. The most important differences are between -2000 and +2000 $\mu\text{g}\cdot\text{m}^{-3}$ in Bodélél. A major forecast underestimation is calculated for the 11 September with -2000 $\mu\text{g}\cdot\text{m}^{-3}$, meaning that an important peak of surface concentrations was modelled for (D-1) and (D+0) but not in advance. In Capo Verde, the surface concentrations are lower, logically after long-range transport. The concentrations remain high with peaks around 700 $\mu\text{g}\cdot\text{m}^{-3}$. It is not the case of 11 September, but peaks are noted on 9, 12 and 16 September mainly. As well as for Bodélél, a large variability is calculated for 11 September, with forecast differences up to -200 $\mu\text{g}\cdot\text{m}^{-3}$. As for Bodélél, the model underestimates the concentrations when the forecast is in advance. In addition to these results, time-series of 2m temperature, 10m wind speed and precipitation are presented in **Appendix A1**.

130 3.2 Maps of mineral dust concentrations and AOD

Maps are presented for surface mineral dust concentrations ($\mu\text{g}\cdot\text{m}^{-3}$) and Aerosol Optical Depth for the 11 September at 12:00 UTC, in **Figure 4**. Note that complementary maps for wind speed and precipitation are presented in **Appendix A2**. The simulation shows a large mineral dust plume, flowing from Africa to northern Atlantic sea. The site of Capo Verde is under

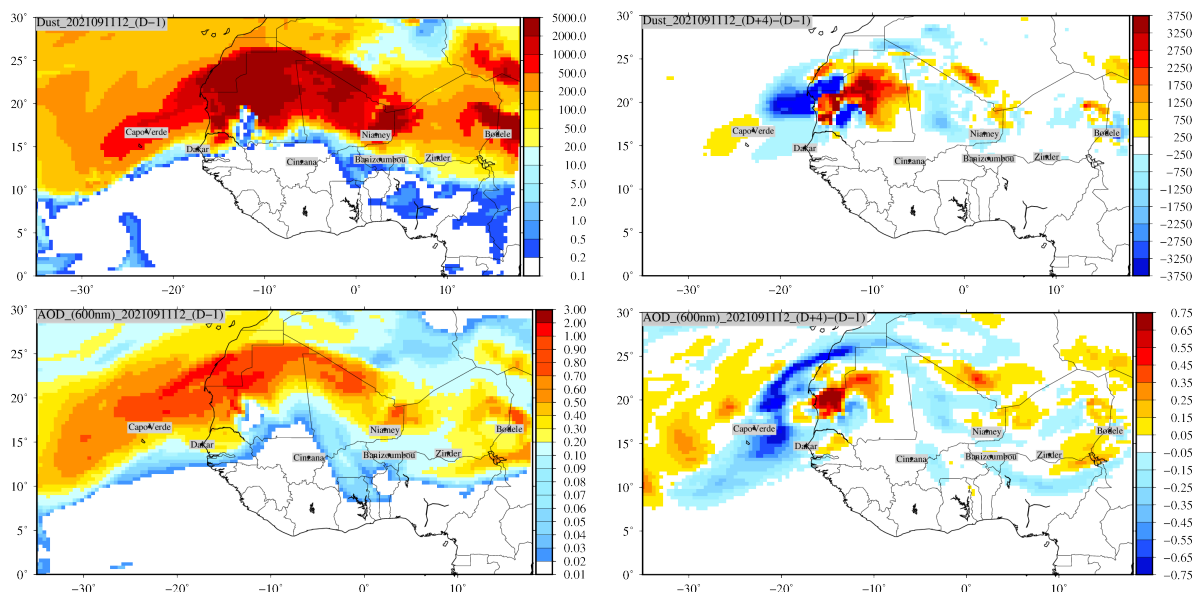


Figure 4. Maps of surface mineral dust concentrations ($\mu\text{g}\cdot\text{m}^{-3}$) and Aerosol Optical Depth for the 11 September at 12:00 UTC. Values are displayed (left) for the forecast lead (D-1) and (right) for the differences between the forecast leads (D+4)-(D-1).

135 this plume and the trajectory over the ocean corresponds to the low wind speed values. The differences show the same kind
of dipole as diagnosed for the precipitation (**Figure A4**), showing that the shift between the forecast leads directly impacts
the surface concentrations. With large positive values over land and negative over the sea, it is noticeable that the more recent
forecast (D-1) diagnose a larger wind speed then transport: the dust plume is more over land for (D+4), but is already arrived
over sea in (D-1). It means that over Capo Verde, the last forecast diagnosed finally more dust concentrations than the previous
forecasts. The Aerosol Optical Depth is the reflect of the mineral dust concentration, even if it diagnoses the radiative effect
140 of all aerosols in the whole atmospheric column. The shape of the plume is slightly different and a larger spatial spread of
the differences between the forecast leads. The differences remain important in absolute values since they can reach ± 0.75
when the maximum of AOD is 2. The variability in the forecast is important and show for this day that the forecast of (D+4)
underestimated AOD over Capo Verde compared to (D-1). In addition to these horizontal maps, the same variables are analyzed
in **Appendix A3** as vertical cross-sections.



145 3.3 Statistical scores

Usually, the variables O_t and M_t stand for the observed and modeled values, respectively, at time t . In case of this study, as we want to quantify the variability of the forecast, the variable O_t is the model realization at (D-1) and the variable M_t is the model realization at leads (D+0) to (D+4). The mean value $\overline{X_N}$ is calculated as:

$$\overline{X_N} = \frac{1}{N} \sum_{t=1}^N X_t \quad (1)$$

150 with N the total number of hours of the simulation. To quantify the temporal variability, the Pearson product moment correlation coefficient R is calculated as:

$$R = \frac{\frac{1}{N} \sum_{t=1}^N (M_t - \overline{M_t}) \times (O_t - \overline{O_t})}{\sqrt{\frac{1}{N} \sum_{t=1}^N (M_t - \overline{M_t})^2 \times \frac{1}{N} \sum_{t=1}^N (O_t - \overline{O_t})^2}}, \quad (2)$$

The spatial correlation, noted R_s , uses the same formula type except it is calculated from the temporal mean averaged values of observations and model for each location where observations are available.

$$155 R_s = \frac{\sum_{i=1}^I (\overline{M_i} - \overline{\overline{M}}) (\overline{O_i} - \overline{\overline{O}})}{\sqrt{\sum_{i=1}^I (\overline{M_i} - \overline{\overline{M}})^2 \sum_{i=1}^I (\overline{O_i} - \overline{\overline{O}})^2}} \quad (3)$$

where I is the number of stations. The normalized Root Mean Square Error, $nRMSE$, is expressed as:

$$nRMSE = \sqrt{\frac{1}{T} \frac{1}{I} \sum_{t=1}^T \sum_{i=1}^I \left(\frac{O_{t,i} - M_{t,i}}{O_{t,i}} \right)^2} \quad (4)$$

for all stations i and all times t .

To quantify the mean differences between the several leads, the bias is also quantified as:

$$160 \text{ bias} = \frac{1}{N} \sum_{t=1}^N (M_t - O_t) \quad (5)$$

Results are presented in **Table 2** for the surface meteorological variables, 10m wind speed and the 2m temperature, and in **Table 3** for the total precipitation and the surface mineral dust concentrations. For each variable, the presented values are the mean value (averaged over the whole month of September 2021), the bias and the correlation. The line (D-1) is always empty since the bias and the correlation of itself compared to (D-1) gives the values of 0 and 1, respectively.

165 For the 10m wind speed, it is noticeable that the mean value does not evolve a lot during the forecast. In Bodélé, the bias is always lower than -0.2 m.s^{-1} , the negative value meaning that the (D-1) analysis simulation was the one with the highest wind



Lead	10m wind speed (m.s^{-1})			2m temperature ($^{\circ}\text{C}$)		
	Mean	Bias	R	Mean	Bias	R
<i>Bodélé</i>						
(D-1)	3.89			32.2		
(D+0)	3.83	-0.060	0.23	32.1	-0.082	0.90
(D+1)	3.72	-0.161	-0.17	32.2	-0.013	0.80
(D+2)	3.78	-0.110	0.06	32.2	-0.023	0.79
(D+3)	3.83	-0.056	0.05	32.0	-0.145	0.75
(D+4)	3.69	-0.199	-0.04	31.9	-0.305	0.79
<i>Capo Verde</i>						
(D-1)	5.49			24.6		
(D+0)	5.56	0.069	0.04	24.6	0.007	0.57
(D+1)	5.55	0.056	-0.27	24.6	0.021	0.16
(D+2)	5.47	-0.021	-0.15	24.6	0.032	0.08
(D+3)	5.54	0.048	0.03	24.6	0.051	0.24
(D+4)	5.38	-0.110	-0.01	24.6	0.036	0.29

Table 2. Statistical scores for the daily averaged 10-m wind-speed (m.s^{-1}) and 2m temperature ($^{\circ}\text{C}$) in Bodélé and Capo Verde.

speed. In Capo Verde, the mean value is larger, but the bias lower. With a maximum of -0.11, and negative or positive values, there is not a lot of variability for this site. An important point is the correlation of the leads compared to the (D-1) one: the values are very low, for the two sites: between -0.27 and 0.27 for the maximum values. It means that, from one day to the next one, the time-series are varying a lot in frequency. If the mean values are close, the maximum of wind speed are not at the same time.

For the 2m temperature, we can also observe an important lack of variability for the mean values. The 2m temperature is higher ($\approx 32^{\circ}\text{C}$ in average) in Bodélé than in Capo Verde ($\approx 24^{\circ}\text{C}$ in average), clearly showing the difference between a desert and a maritim air around an Island. The bias is negative over Bodélé showing that the forecast tends to underestimate the temperature compared to the lead (D-1). The bias is positive over Capo Verde but the values are so low that it is negligible. Over Bodélé, the correlation remains high (between 0.75 and 0.9) showing that the forecast over the desert is very stable. It is not the case over Capo Verde, with a large variability, between 0.08 and 0.57. And the decrease of the correlation is not linear with the increasing lead: (D+4) has a correlation of 0.29 when (D+2) has a correlation of 0.08. The fact to have a stable forecast over land does not mean that the forecast is stable over the Atlantic sea, the meteorological systems being completely different.

The same type of scores is displayed in Table 3 for the daily cumulated total precipitation ($\text{kg.m}^{-2}.\text{h}^{-1} \times 100$) and the surface mineral dust concentrations ($\mu\text{g.m}^{-3}$) in Bodélé and Capo Verde. For the precipitation, it is remarkable to see that the correlation is always close to zero. It means that, from day to day, the precipitation varies a lot for a specific location. It is logical since precipitation is a threshold process, not continuous in space and time, contrarily to the temperature or the wind.



Lead	Total precipitation ($\text{kg}\cdot\text{m}^{-2}\cdot\text{h}^{-1} \times 100$)			Mineral dust conc. ($\mu\text{g}\cdot\text{m}^{-3}$)		
	Mean	Bias	R	Mean	Bias	R
<i>Bodélé</i>						
(D-1)	1.14			1291.0		
(D+0)	1.12	-0.021	0.02	1248.9	-42.111	0.17
(D+1)	0.70	-0.443	-0.02	1125.9	-165.070	-0.09
(D+2)	0.86	-0.283	-0.04	1290.4	-0.584	-0.10
(D+3)	0.28	-0.861	-0.04	1352.2	61.142	-0.22
(D+4)	1.92	0.776	-0.06	1206.6	-84.424	-0.13
<i>Capo Verde</i>						
(D-1)	2.81			195.6		
(D+0)	2.51	-0.305	0.00	200.3	4.703	0.13
(D+1)	3.12	0.304	-0.07	197.9	2.336	-0.30
(D+2)	2.53	-0.286	-0.06	193.1	-2.446	0.14
(D+3)	6.43	3.612	-0.06	185.5	-10.045	0.19
(D+4)	3.25	0.434	-0.07	173.5	-22.108	-0.11

Table 3. Statistical scores for the daily cumulated total precipitation ($\text{kg}\cdot\text{m}^{-2}\cdot\text{h}^{-1} \times 100$) and surface mineral dust concentrations ($\mu\text{g}\cdot\text{m}^{-3}$) in Bodélé and Capo Verde.

The bias is important, both in Bodélé and Capo Verde: it corresponds to the fact to have a forecast with a precipitation and
 185 the next lead without for the same place and time. For this process, the statistical scores show that the forecast is very variable
 from one day to another.

For the mineral dust concentrations, the correlation is also low for both sites. Over Bodélé, the values are between -0.22 for
 (D+3) and +0.17 for (D+0), and over Capo Verde, values are between -0.30 for (D+1) and +0.19 for (D+3). The bias is non
 negligible and may reach 10% of the mean values. As for the other parameters, there is no a regular decrease with an increasing
 190 lead: the system is chaotic and the unstability of the forecast for dust concentrations is the reflect of the unstability of the mean
 wind speed over sources areas, then emissions, then transport, then concentrations at remote locations. The only stable point is
 that, considered together, the bias and the correlation are the best for (D+1), logically the first day of forecast, thus relatively
 close to (D-1).

4 Merging the forecast leads to make an ensemble

195 The previous results showed that small variations of meteorological variables may change a lot mineral dust concentrations
 after long-range transport. This quantification was made with only model results in order to quantify the model's variability.



For some locations, it is however possible to compare the AOD to AERONET measurements. During the studied period, four stations are present in the modelled domain and have available data: Zinder (Niger), Banizoumbou (Niger), Cinzana (Mali) and Capo Verde. Note that, unfortunately, there is no measurement for this period at Bodélé. Using these data, it is possible to calculate statistical scores between the modelled forecast and the measurements.

An added value in this study, it that it is also possible to add two model realizations. Considering that the various forecast leads are performed each time with a new meteorology, then natural emissions (here mineral dust emissions), we can consider all these leads as independant simulations. They are thus similar to ensemble forecast members, usually made the same day but with perturbed initial conditions. As presented in **Figure 2**, for one date we have six simulations. It is possible to make the hypothesis that these six forecast leads are equivalent to six ensemble members. To test this approach, we use the time-series at the four locations where AERONET measurements are available to create a two new sets called ENSmean and ENS median:

- ENSmean corresponds to the mean averaged value of the six members,
- ENSmedian corresponds to the median of the members. Having only size members, this values is in fact the mean average of the 3th and 4th members.

4.1 Scores during the CADDIWA period

Statistical scores are first calculated for the period of the CADDIWA experiment, from 1st to 31th September 2021. Results are presented in **Table 4**. For each site and each parameter (correlation R , nRMSE or bias), the best score is bolded. It shows that model realizations are close from each other but remain different to the measurements. The variability of the forecast is lower than the difference between measurements and models. It means that the model systematically underestimates the AOD whatever the perturbations included in each forecast realization. The bias is negative for all sites over land (Zinder, Banizoumbou and Cinzana) and over sea, the island of Capo Verde. The bias is smaller over this latter site.

For the correlation, the best value is obtained for the ENSmean lead for two sites on four: Capo Verde and Zinder. For Cinzana and Banizoumbou the best correlation is obtained for (D+3) and (D+2), respectively. It means that (i) the best scores is not for the "analysis" lead (D-1) as it could be expected, (ii) the combination of lead leading to ENS may be the best forecast. For the bias, results are different: the lower biases are not for ENS. In Capo Verde, the lower bias is for (D-1). For the other sites, they are for (D+3) and (D+4) forecasts. Note that even if ENS has not the best score, it is no the worse too. These scores show that best forecast lead is not always the more close to the analysis. It also show that the use of a "ensemble" lead may provide good results.

For the nRMSE, some best scores are laos obtained for the ENSmean and ENSmedian configurations, showing that the merge of the lead may reduce the model error. For the bias, the values remain very close from one lead to antoher and there is no really a best configuration.

Table 5 summarizes the results presented in **Table 4** by recalculating the scores but for the four stations together. As for the previous results. the best scores are bolded as a function of the forecast lead. The spatial correlation is the best for (D+3) but the correlation and the nRMSE are the best for the ENSmean forecast. The bias remains the same for all model realizations.



SITE	<i>obs</i>	<i>model</i>	R	nRMSE	bias
<i>(D-1)</i>					
CapoVerde	0.41	0.33	0.75	0.49	-0.07
Cinzana	0.28	0.11	0.44	0.66	-0.18
Banizoumbou	0.43	0.13	0.76	0.68	-0.30
Zinder	0.55	0.26	0.54	0.51	-0.29
<i>(D+0)</i>					
CapoVerde	0.41	0.33	0.75	0.49	-0.07
Cinzana	0.28	0.11	0.45	0.66	-0.18
Banizoumbou	0.43	0.13	0.76	0.68	-0.30
Zinder	0.55	0.26	0.55	0.51	-0.29
<i>(D+1)</i>					
CapoVerde	0.41	0.33	0.76	0.49	-0.08
Cinzana	0.28	0.10	0.43	0.68	-0.18
Banizoumbou	0.43	0.14	0.74	0.66	-0.30
Zinder	0.55	0.26	0.46	0.51	-0.29
<i>(D+2)</i>					
CapoVerde	0.41	0.32	0.76	0.51	-0.08
Cinzana	0.28	0.11	0.36	0.66	-0.18
Banizoumbou	0.43	0.14	0.76	0.67	-0.30
Zinder	0.55	0.27	0.52	0.52	-0.28
<i>(D+3)</i>					
CapoVerde	0.41	0.30	0.78	0.52	-0.11
Cinzana	0.28	0.12	0.48	0.61	-0.16
Banizoumbou	0.43	0.14	0.68	0.66	-0.29
Zinder	0.55	0.27	0.49	0.50	-0.27
<i>(D+4)</i>					
CapoVerde	0.41	0.32	0.67	0.59	-0.09
Cinzana	0.28	0.13	0.35	0.65	-0.15
Banizoumbou	0.43	0.17	0.39	0.64	-0.27
Zinder	0.55	0.23	0.56	0.56	-0.32
<i>Mean</i>					
CapoVerde	0.41	0.32	0.78	0.49	-0.08
Cinzana	0.28	0.11	0.45	0.64	-0.17
Banizoumbou	0.43	0.14	0.75	0.64	-0.29
Zinder	0.55	0.26	0.59	0.50	-0.29
<i>Median</i>					
CapoVerde	0.41	0.33	0.76	0.49	-0.08
Cinzana	0.28	0.11	0.43	0.65	-0.18
Banizoumbou	0.43	0.14	0.75	0.67	-0.30
Zinder	0.55	0.26	0.55	0.50	-0.29

Table 4. For the period 1st to 31th September 2021, correlation (R), nRMSE and bias calculated between the AERONET Aerosol Optical Depth measurements and the modelled results. Results are presented for four sites, Capo Verde, Cinzana, Banizoumbou and Zinder and for six forecast leads, from (D-1) to (D+4). Two additional forecast leads called ENSmean and ENSmedian represent the mean average of the previous six leads and the median, respectively. The best scores for each sites and among all leads are bolded.



Lead	R_s	R	nRMSE	bias
(D-1)	0.53	0.62	0.58	-0.21
(D+0)	0.53	0.63	0.58	-0.21
(D+1)	0.57	0.60	0.58	-0.21
(D+2)	0.60	0.60	0.59	-0.21
(D+3)	0.62	0.61	0.57	-0.21
(D+4)	0.45	0.49	0.61	-0.21
ENSmean	0.57	0.64	0.57	-0.21
ENSmedian	0.54	0.62	0.58	-0.21

Table 5. For the period 1st to 31th September 2021, spatial and temporal correlation, nRMSE and bias for each lead and as average for the four stations.

230 4.2 Scores during the extended forecast period

In order to have more statistically robust results, the complete modelled period is now presented: from 15th August to 1st November 2021. This period is around the CADDIWA experiment and just correspond to the period when the forecast system was running. It corresponds to 2.5 months. Results are presented as time-series in **Figure 5** for the daily averaged AOD.

It is noticeable that the month of September (compared to August and October) is not the month with more AOD: values
235 are of the same order of magnitude over the whole period. Except in Capo Verde where the largest peaks are observed during September 2021, corresponding to the CADDIWA measurements campaign.

Statistical scores are presented in **Table 6** in the same way that in **Table 4** but this time for a longer period. Over this period, the availability of hourly measurements is 62.5%, 77.8%, 79.2% and 77.8% for Capo Verde, Cinzana, Banizoumbou and Zinder stations, respectively. For this longer period, the best correlation are not for the ensemble leads, except for the
240 nRMSE in Capo Verde and Zinder and for the bias in Capo Verde. For the correlation, the best scores are now for the first forecast leads, i.e (D-1) and (D+0). All in all, the scores are very close from one lead to the next one.

Table 7 summarizes the results presented in **Table 6** as in **Table 5**. The best spatial correlation is again for (D+3) when the best temporal correlation is obtained for the leads (D-1) and (D+0). For the nRMSE, scores are very close between leads, and the best values are for (D-1), (D+0), (D+1) but also for the ensemble, both with ENSmean and ENSmedian.

245 5 Conclusions

In this study, the first goal was to examined the variability of the forecast. This forecast was daily performed for six days, during the period August to October 2021 and as support for the CADDIWA field campaign. For meteorological variables (2m temperature, 10m wind speed, total precipitation rate) and surface concentrations of mineral dust, the variability from day to day was quantified. Two sites were compared, Bodélé (desert area and important source of dust) and Capo Verde (where the

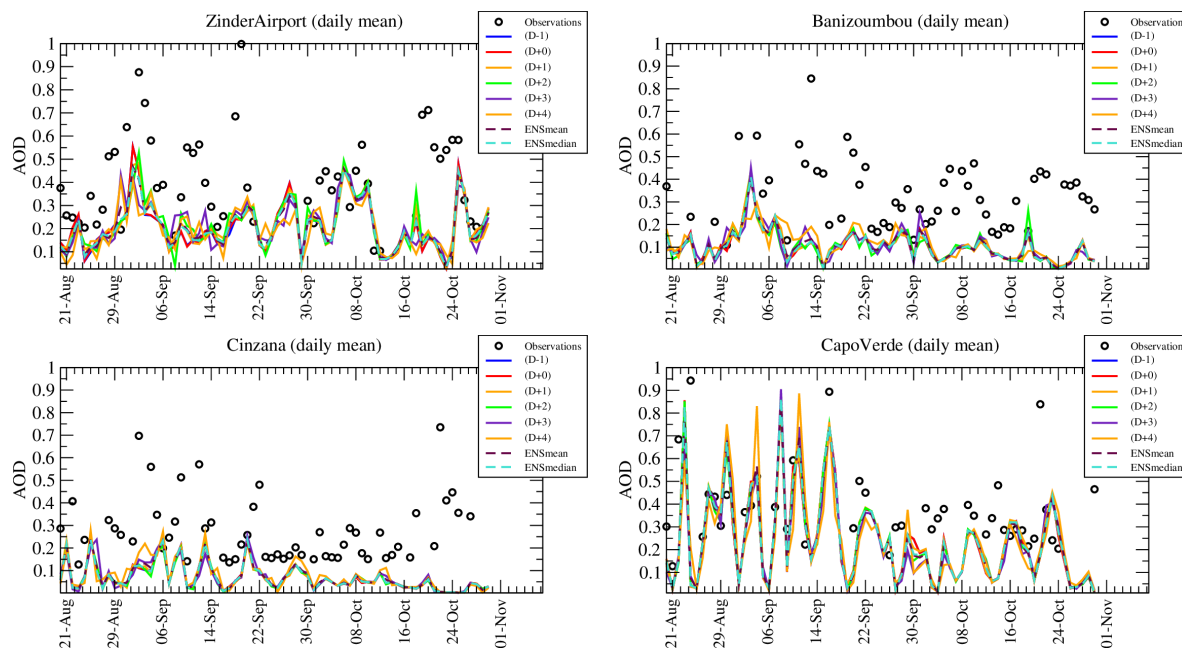


Figure 5. Time-series of Aerosol Optical Depth (AOD) measured by AERONET and modelled during the forecast and for several leads. The last time-series, called ENSmean and ENSmedian, are the mean averaged and the median values of the previous leads, from (D-1) to (D+4).

250 measurements of DACCIWA were coordinated). It has been shown that the wind speed is highly variable in forecast when the temperature is stable over land but also variable over sea (Capo Verde being a group of little Islands). The less stable parameter is the precipitation at one location when the model may forecast an event one day and not at all the day after (and vice-versa). One goal of the study was to examine if a large forecast variability at one site (such as Bodélé) may have a visible impact at a downwind remote site (such as Capo Verde): no evidence was found of a transport of variability (or a transport of stability) during the forecast. Having an important variability for wind speed, precipitation and temperature, a large variability was also diagnosed for the surface concentration of mineral dust. Between forecast leads, large differences were found both for the correlation and the bias. Knowing the model configuration used for this study (no direct and indirect effects of aerosols on meteorology and only mineral dust as natural emissions), the diagnosed variability is large but may be underestimated. A next study could be to replay this forecast but with a complete model version (i.e all anthropogenic and natural emissions included by default in the CHIMERE model) and a validation with the measurements of the experiment to come.

260 Second, a new way to combine forecast leads was tested. Considering that several forecast leads may be considered as the members of an ensemble, they are combined from (D-1) to (D+4) for all coinciding dates. Two calculations are tested: with the mean averaged value and the median. These new "forecast leads" are compared, with all others, to the Aerosol Optical Depth measurements of AERONET. Correlation, nRMSE and bias are calculated between observations and measurements. It is noticeable there is no steady decline in the quality of the scores the further into the forecast we go. But it is also notable



SITE	<i>obs</i>	<i>model</i>	R	nRMSE	bias
<i>(D-1)</i>					
CapoVerde	0.41	0.28	0.48	0.56	-0.13
Cinzana	0.29	0.07	0.41	0.76	-0.22
Banizoumbou	0.36	0.11	0.60	0.69	-0.25
Zinder	0.44	0.22	0.42	0.52	-0.22
<i>(D+0)</i>					
CapoVerde	0.41	0.28	0.48	0.56	-0.13
Cinzana	0.29	0.07	0.41	0.76	-0.22
Banizoumbou	0.36	0.11	0.60	0.69	-0.25
Zinder	0.44	0.22	0.42	0.52	-0.22
<i>(D+1)</i>					
CapoVerde	0.41	0.28	0.48	0.56	-0.13
Cinzana	0.29	0.07	0.41	0.77	-0.22
Banizoumbou	0.36	0.11	0.60	0.69	-0.25
Zinder	0.44	0.22	0.37	0.51	-0.22
<i>(D+2)</i>					
CapoVerde	0.41	0.27	0.49	0.56	-0.13
Cinzana	0.29	0.07	0.36	0.76	-0.21
Banizoumbou	0.36	0.11	0.56	0.70	-0.25
Zinder	0.44	0.23	0.40	0.52	-0.22
<i>(D+3)</i>					
CapoVerde	0.41	0.26	0.42	0.58	-0.15
Cinzana	0.29	0.08	0.34	0.74	-0.21
Banizoumbou	0.36	0.12	0.50	0.70	-0.24
Zinder	0.44	0.23	0.31	0.56	-0.21
<i>(D+4)</i>					
CapoVerde	0.41	0.26	0.41	0.61	-0.15
Cinzana	0.29	0.09	0.24	0.74	-0.20
Banizoumbou	0.36	0.12	0.36	0.68	-0.24
Zinder	0.44	0.21	0.30	0.61	-0.23
<i>Mean</i>					
CapoVerde	0.41	0.27	0.48	0.56	-0.14
Cinzana	0.29	0.08	0.38	0.75	-0.21
Banizoumbou	0.36	0.11	0.58	0.68	-0.25
Zinder	0.44	0.22	0.41	0.52	-0.22
<i>Median</i>					
CapoVerde	0.41	0.28	0.48	0.56	-0.13
Cinzana	0.29	0.07	0.39	0.76	-0.22
Banizoumbou	0.36	0.11	0.59	0.69	-0.25
Zinder	0.44	0.22	0.39	0.51	-0.22

Table 6. For the period 15th August to 1st November 2021, correlation (R), nRMSE and bias calculated between the AERONET Aerosol Optical Depth measurements and the modelled results. Results are presented for four sites, Capo Verde, Cinzana, Banizoumbou and Zinder and for six forecast leads, from (D-1) to (D+4). Two additional forecast leads called ENSmean and ENSmedian represent the mean average of the previous six leads and the median, respectively. The best scores for each sites and among all leads are bolded.

that out of four sites, the best scores for two sites are with the ensemble for the period of the CADDIWA campaign. It is not the case for an extended analyzed period, highlighting that the scores are close form one lead to another. The 'ensemble



Lead	R_s	R	nRMSE	bias
(D-1)	0.87	0.48	0.63	-0.20
(D+0)	0.87	0.48	0.63	-0.20
(D+1)	0.87	0.46	0.63	-0.20
(D+2)	0.90	0.45	0.64	-0.20
(D+3)	0.91	0.39	0.64	-0.20
(D+4)	0.86	0.33	0.66	-0.20
ENSmean	0.87	0.46	0.63	-0.20
ENSmedian	0.87	0.46	0.63	-0.20

Table 7. For the period 15th August to 1st November 2021, spatial and temporal correlation, nRMSE and bias for each lead and as average for the four stations.

methodology provides the best scores when the AOD values are the most important and the most variables in time. This result opens perspectives for forecasting. It would be interesting to test this hypothesis on operational systems: if the combination of the previous forecasts allows to improve the initial conditions of a new forecast, it would allow to realize less ensemble simulations for the same day and thus to reduce considerably the cost of forecast calculation.

Appendix A: Complementary analysis with the meteorological variables

A1 Time-series of meteorological variables

In addition to the time-series presented in Section 3.1, the same results are here presented for 2m temperature, 10m wind speed and precipitation rate.

Figure A1 presents time-series and differences for 2m temperature ($^{\circ}\text{C}$) in Bodélé and Capo Verde. The 11 and 18 September are noted on the Figure with a black vertical line. In Bodélé the temperature is higher than in Capo Verde, with values between 30 and 35 $^{\circ}\text{C}$. During the month of September the temperature decreases regularly. The days of 11 and 18 September correspond to periods with the highest temperature values. In Capo Verde, there is no similar trend: the daily averaged temperature remains around 25 $^{\circ}\text{C}$ showing the maritime characteristic of the Capo Verde environment. The differences are low and oscillate between -2 and +2 $^{\circ}\text{C}$. The longer the forecast, the greater the variability. In Capo Verde, the variability is lower and between -1 and +1 $^{\circ}\text{C}$. As in Bodélé, the largest differences with (D-1) are obtained with (D+4). The forecast of temperature appear to be relatively stable, the differences logically growing with the increasing leads.

Figure A2 presents results for 10m wind speed. Values are lower in Bodélé (middle of desert) than in Capo Verde (an island). In Bodélé, daily averaged values are between 2 and 7 $\text{m}\cdot\text{s}^{-1}$, values lower than minimum value generally required for dust erosion over barren soils. But hourly values may be larger and the model uses a Weibull distribution to take into account the sub-hour and the sub-grid spatial variability, (Menut, 2018). It is noticeable the two days of 11 and 18 September don't

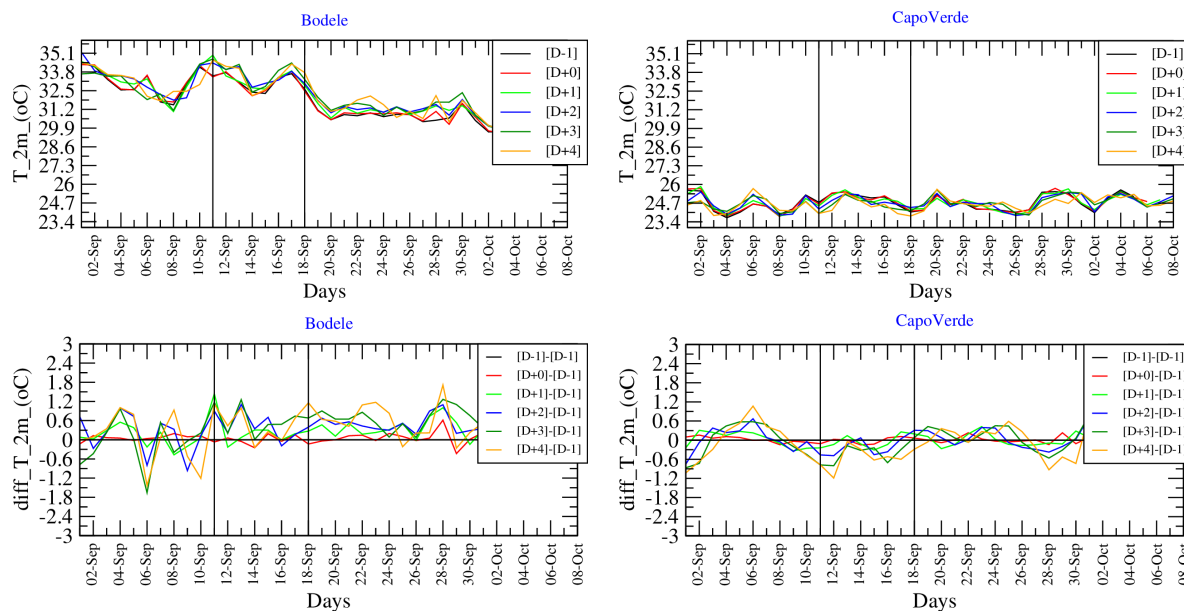


Figure A1. Time-series of 2m temperature ($^{\circ}\text{C}$) for each lead and of differences between leads.

correspond to high wind speed value, as well as the days before. In Capo Verde, the wind speed values are between 3 and 10 $\text{m}\cdot\text{s}^{-1}$, with day to day variability higher than in Bodélél. Some days shows high values such as 5 and 11 September. It is the signature, close to the surface, to large scale meteorological motions.

On **Figure A2**, differences are also presented. Differences are of the same order of magnitude between the two locations. For (D+0)-(D-1), differences are of maximum $\pm 0.5 \text{ m}\cdot\text{s}^{-1}$, when higher values are calculated for (D+4)-(D-1) with maximum around $\pm 3 \text{ m}\cdot\text{s}^{-1}$. It is noticeable that the differences increase with the lead: the more distant the forecast, the greater the difference between the leads. For these differences, there is no systematic bias: they can be negative or positive, showing a variability not due to large scale and/or persistent atmospheric systems, but much more regional variability, with an higher temporal frequency. More specifically for the 11 September, when the absolute values shows a peak in Capo Verde, the differences show this peak was predicted late: four days before, (D+4) forecast, the peak is $6 \text{ m}\cdot\text{s}^{-1}$, when it is $9 \text{ m}\cdot\text{s}^{-1}$ for (D+0). The difference is then $-3 \text{ m}\cdot\text{s}^{-1}$, one of the most important during the whole modelled period.

Figure A3 presents the same kind of time-series but for total precipitation in $\text{kg}\cdot\text{m}^{-2}\cdot\text{h}^{-1} \times 100$. The time series show that only a few periods had precipitation episodes for the two sites of Bodélél and Capo Verde. In Bodélél, the two periods with rain are the 6 and 15 September. In Capo Verde, three episodes are modelled, 6, 14 September and 5 October (the last one being out of the current analyzed period). For the first episode in Bodélél, 6 September, it appears only for the forecast lead (D+4). For the other forecasts, closer in time, there is no precipitation. For the second episode, a time variability is observed: depending on the lead, the precipitation have similar magnitude but is forecasted on 14, 15 or 16 September. The difference show the forecast is mostly overestimated compared to the analysis of (D-1). In Capo Verde, the several precipitation episodes are also varying

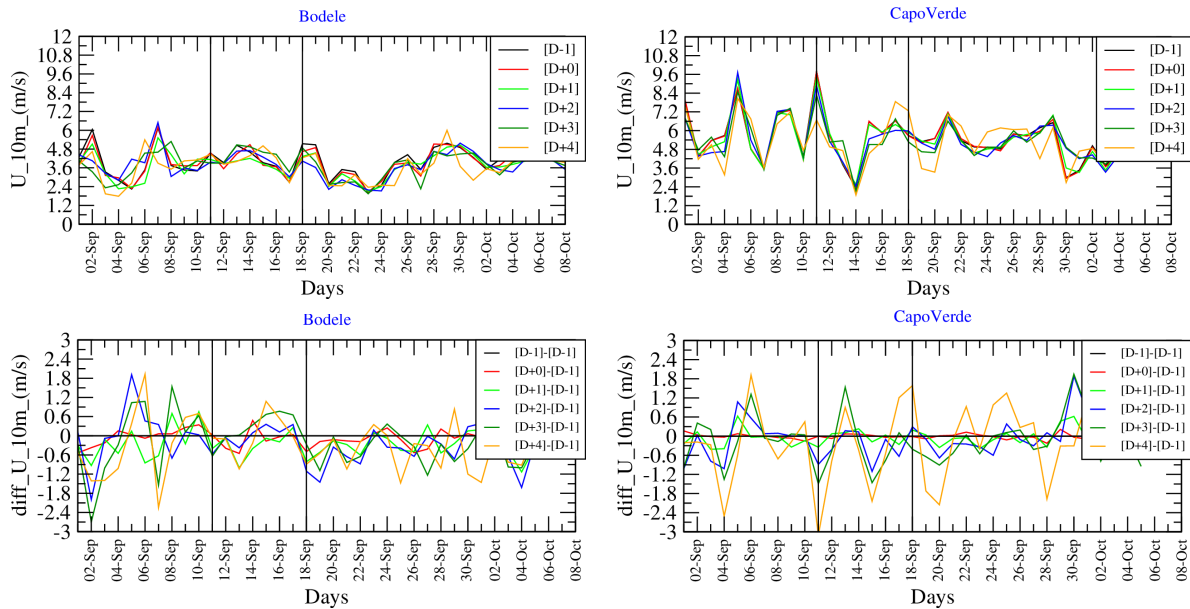


Figure A2. Time-series of 10m wind speed ($\text{m}\cdot\text{s}^{-1}$) for each lead and of differences between leads.

in time. If the first episode is over-estimated for the (D+4) lead, it is finally underestimated by the other leads, from (D+1) to (D+3). The second episode is forecasted with less variability in time, all forecasts being for the 13 or 14 September only. The magnitudes are close between leads, with only a low underestimation compared to (D-1). Finally, the forecast is less variable in Capo Verde than in Bodélé.

310 A2 Maps of wind speed and precipitation

Results are presented as maps for one date, the 11 September at 12:00 UTC. **Figure A4** first presents maps for the 10-m wind-speed ($\text{m}\cdot\text{s}^{-1}$) and total precipitation ($\text{kg}\cdot\text{m}^{-2}\cdot\text{h}^{-1}$). On the left panel, the absolute value of the forecast lead (D-1) is presented. On the right panel, the differences between the leads (D-4) and (D-1). Note that for the wind speed, the wind vectors are superimposed. For the 10 m wind speed, the values of (D-1) show moderate values (between 0 and 3 $\text{m}\cdot\text{s}^{-1}$), except over
 315 Mauritania with maximum values $\approx 15 \text{ m}\cdot\text{s}^{-1}$. The wind speed is larger over the Atlantic sea with values $\approx 8 \text{ m}\cdot\text{s}^{-1}$ near Capo Verde. The Capo Verde site is inbetween two different air masses: one coming from the South and evolving along the African coast, the second one, on the west side of Capo Verde and coming from the North. It results of low wind locally in Capo Verde. The map of differences show the same pattern, meaning that this structure changes during the forecast: the (D+4) forecast shows negative values, meaning that the wind speed is higher for (D-1) than (D+4). It means that the strong gradient,
 320 from north-east to south-west and flewing over Capo Verde, observed for (D-1), was not present for the forecast four days in advance.

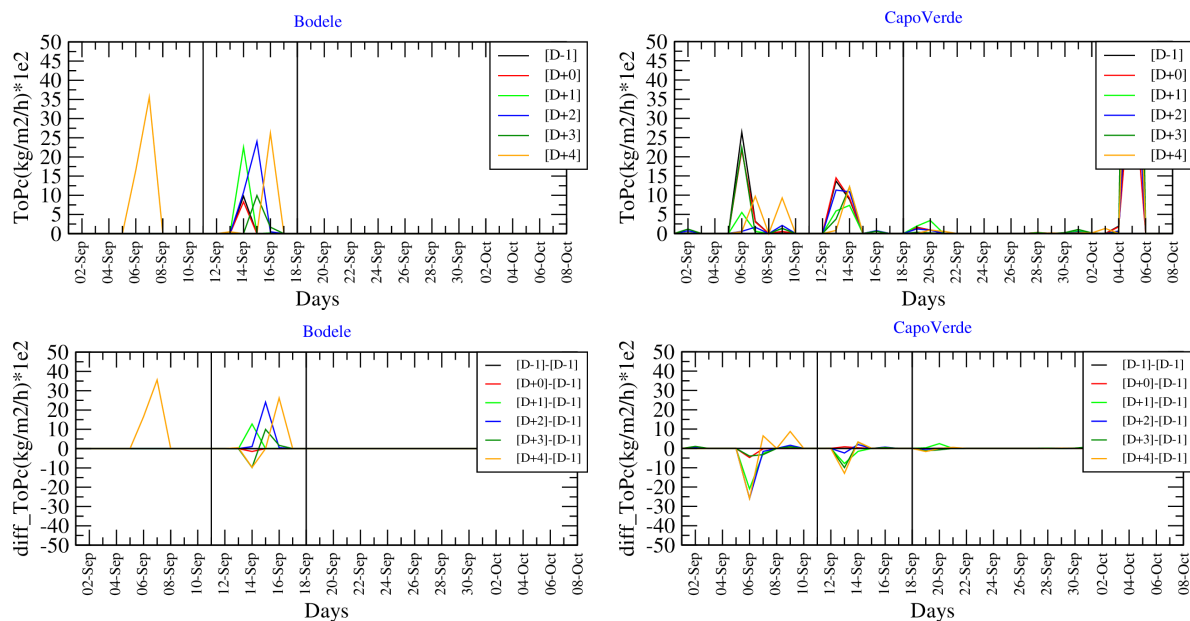


Figure A3. Time-series of total precipitation ($\text{kg}\cdot\text{m}^{-2}\cdot\text{h}^{-1} \times 100$) for each lead and of differences between leads.

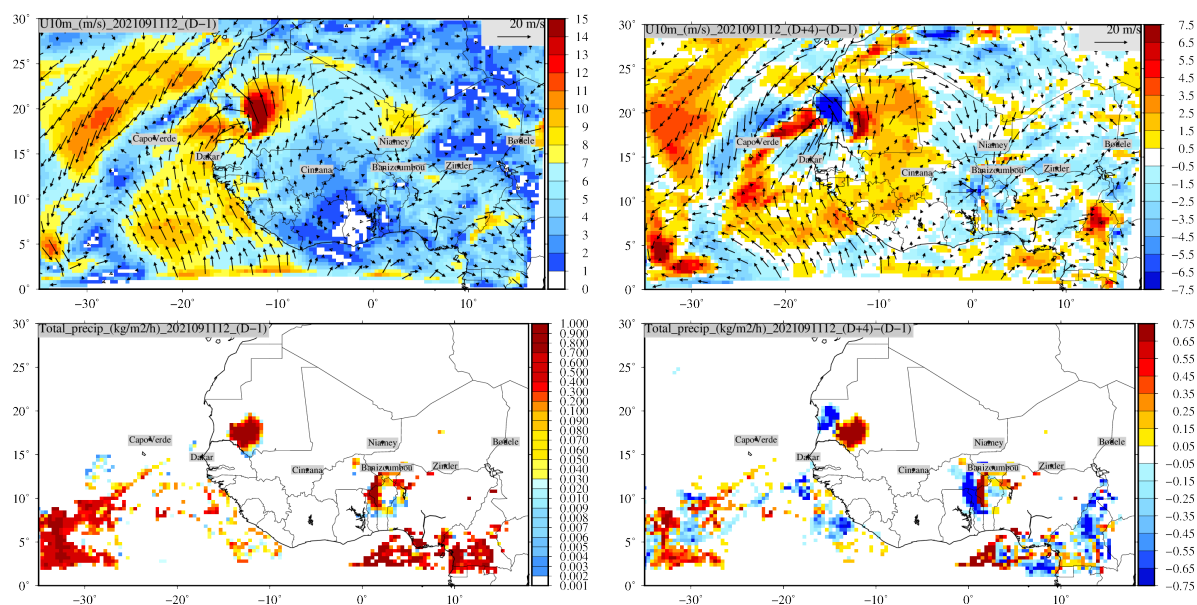


Figure A4. Maps of 10-m wind-speed ($\text{m}\cdot\text{s}^{-1}$) and total precipitation ($\text{kg}\cdot\text{m}^{-2}\cdot\text{h}^{-1}$) for the 11 September at 12:00 UTC. Values are displayed (left) for the forecast lead (D-1) and (right) for the differences between the forecast leads (D+4)-(D-1).



For the total precipitation, **Figure A4**, the results on the map show very localized events. Over Africa and over Mauritania, the large amount of precipitations ($\approx 1 \text{ kg}\cdot\text{m}^{-2}\cdot\text{h}^{-1}$) is colocated with the large 10 m wind speed values. Other precipitation events are modelled more in the South, both over the Atlantic Sea and the Gulf of Guinea, for a latitude below 10°N . The differences map shows negative and positive values: it is the mark of a change in wind speed and direction, then location of the precipitation. But whatever the location, each time a precipitation was forecasted, each time it occurred, even if this is not strictly at the same place. For this day, no precipitation was forecasted over Capo Verde and this forecast remained stable during the several forecast leads.

A3 Vertical cross-sections of mineral dust concentrations and rain

Figure A5 presents vertical cross-section of mineral dust concentrations ($\mu\text{g}\cdot\text{m}^{-3}$) and precipitation rate (in $\text{kg}\cdot\text{kg}^{-1}\cdot 10^6$) at isolatitude 17°N for the forecast lead of (D-1) and the difference between (D+4) and (D-1). The same day and hour, than for the horizontal maps, are selected for these results.

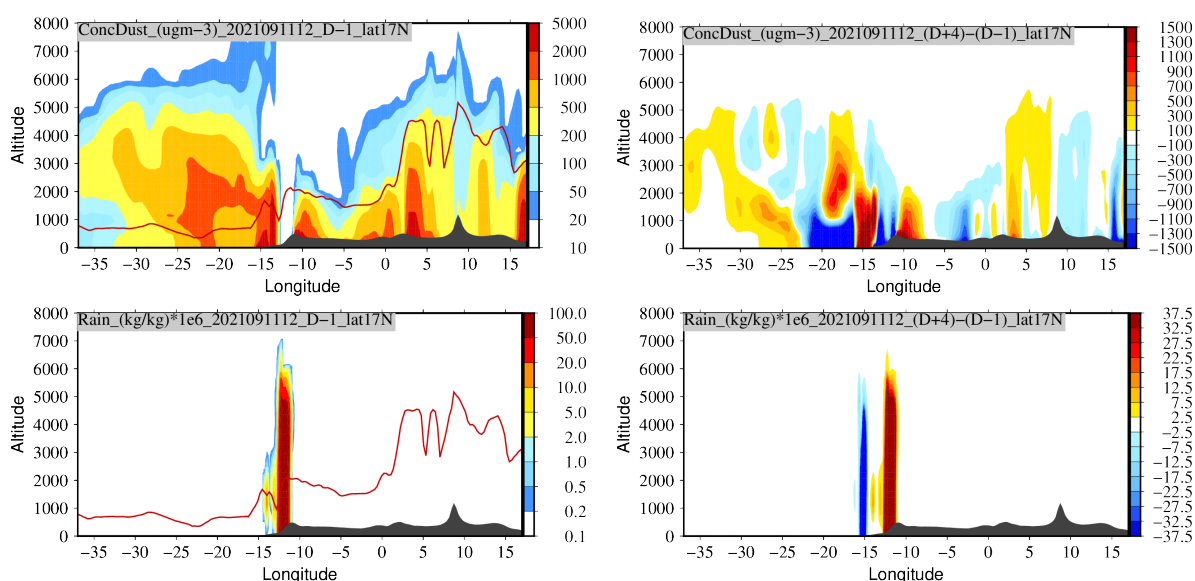


Figure A5. Vertical cross-section of mineral dust concentrations ($\mu\text{g m}^{-3}$) and precipitation rate (in $\text{kg}\cdot\text{kg}^{-1}\cdot 10^6$) at isolatitude 17°N . Figures represent the same date, 11 September 2021 at 12:00 UTC. [left] absolute values for forecast lead (D-1) and [right] differences between forecast leads (D+4)-(D-1). The line in red is the boundary layer height.

The goal of these Figures is to present the vertical extent of the possible differences between the leads. For the mineral dust concentrations, the large surface concentrations extend vertically until 3000 m. And concentrations are non negligible until 7000 m. At the longitude of Capo Verde, -23°W , dust concentrations are large, but the forecast is very variable. The differences shows maximum values between -20 and -10°W . Around -20°W , the vertical structure shows negative values close to the surface but positive values between 1500 and 3000 m, above the boundary layer. It means that the wind direction changed



between the forecast leads but also the vertical distribution of the dust plume coming from Africa. It explains the differences for the surface concentrations and should also have an impact on AOD (see section 4).

340 The vertical profile of rain shows for this day a large event at longitude $\approx -13^\circ\text{W}$. It corresponds to the event seen on **Figure A4** over the south-west of Mauritania. The vertical cross-section of differences shows negative then positive values: the wind being faster as the forecast is close from the current day, the precipitation is transported faster and then appears as positive for longitude -13°W and negative in longitude -16°W . If the horizontal transport is changing with leads, the vertical structure remains the same with a maximum at 6000 m.

345 *Code availability.* The CHIMERE v2020 model is available on its dedicated web site <https://www.lmd.polytechnique.fr> and for download at <https://doi.org/10.14768/8afd9058-909c-4827-94b8-69f05f7bb46d>.

Data availability. All data used in this study, as well as the data required to run the simulations, are available on the CHIMERE web site download page <https://doi.org/10.14768/8afd9058-909c-4827-94b8-69f05f7bb46d>.

Author contributions. The author made completely the study.

350 *Competing interests.* The author declares that he has no conflict of interest.

Acknowledgements. The authors thank the OASIS modeling team for their support with the OASIS coupler, the WRF developers team for the free use of their model. We thank the investigators and staff who maintain and provide the AERONET data (<https://aeronet.gsfc.nasa.gov/>).



References

- Alfaro, S. C. and Gomes, L.: Modeling mineral aerosol production by wind erosion: Emission intensities and aerosol size distribution in
355 source areas, *J. Geophys. Res.*, 106, 18,075–18,084, 2001.
- Atger, F.: The skill of ensemble prediction systems, *Mon. Wea. Rev.*, 127, 1941–1953, 1999.
- Benedetti, A., Reid, J. S., Knippertz, P., Marsham, J. H., Di Giuseppe, F., Rémy, S., Basart, S., Boucher, O., Brooks, I. M., Menut, L., Mona,
L., Laj, P., Pappalardo, G., Wiedensohler, A., Baklanov, A., Brooks, M., Colarco, P. R., Cuevas, E., da Silva, A., Escribano, J., Flemming,
J., Huneus, N., Jorba, O., Kazadzis, S., Kinne, S., Popp, T., Quinn, P. K., Sekiyama, T. T., Tanaka, T., and Terradellas, E.: Status and future
360 of numerical atmospheric aerosol prediction with a focus on data requirements, *Atmospheric Chemistry and Physics*, 18, 10 615–10 643,
<https://doi.org/10.5194/acp-18-10615-2018>, 2018.
- Bowler, N. E., Arribas, A., and Mylne, K. R.: The Benefits of Multianalysis and Poor Man’s Ensembles, *Monthly Weather Review*, 136,
4113 – 4129, <https://doi.org/10.1175/2008MWR2381.1>, 2008.
- Buizza, R., Richardson, D. S., and Palmer, T. N.: Benefits of increased resolution in the ECMWF ensemble system and comparison with poor-
365 man’s ensembles, *Quarterly Journal of the Royal Meteorological Society*, 129, 1269–1288, [https://doi.org/https://doi.org/10.1256/qj.02.92.](https://doi.org/https://doi.org/10.1256/qj.02.92.2003)
2003.
- Craig, A., Valcke, S., and Coquart, L.: Development and performance of a new version of the OASIS coupler, OASIS3-MCT_3.0, *Geoscientific
Model Development*, 10, 3297–3308, <https://doi.org/10.5194/gmd-10-3297-2017>, 2017.
- Delle Monache, L., Deng, X., Zhou, Y., and Stull, R.: Ozone ensemble forecasts: 1. A new ensemble design, *J. Geophys. Res.*, 111, D05 307,
370 <https://doi.org/10.1029/2005JD006310>, 2006.
- Ebert, E. E.: Ability of a Poor Man’s Ensemble to Predict the Probability and Distribution of Precipitation, *Monthly Weather Review*, 129,
2461 – 2480, [https://doi.org/10.1175/1520-0493\(2001\)129<2461:AOAPMS>2.0.CO;2](https://doi.org/10.1175/1520-0493(2001)129<2461:AOAPMS>2.0.CO;2), 2001.
- Flamant, C., Chaboureau, J., Delanoe, J., Gaetani, M., Jamet, C., Lavaysse, C., Bock, O., Borne, M., Cazenave, Q., Coutris, P., Cuesta,
J., Menut, L., Aubry, C., Benedetti, A., Bossler, P., Bounissou, S., Caudoux, C., Collomb, H., Donal, T., Febvre, G., Fehr, T., Fink, A.,
375 Formenti, P., Araujo, N. G., Knippertz, P., Lecuyer, E., Andrade, M. N., Langué, C. G. N., Jonville, T., Schwarzenboeck, A., and Takeishi,
A.: Cyclogenesis in the tropical Atlantic: First scientific highlights from the Clouds-Atmospheric Dynamics-Dust Interactions in West
Africa (CADDIWA) field campaign, *BAMS*, pp. 1–27, submitted, 2022.
- Halperin, D. J., Penny, A. B., and Hart, R. E.: A Comparison of Tropical Cyclone Genesis Forecast Verification from Three Global Forecast
System (GFS) Operational Configurations, *Weather and Forecasting*, 35, 1801–1815, <https://doi.org/10.1175/waf-d-20-0043.1>, 2020.
- 380 Holben, B., Tanre, D., Smirnov, A., Eck, T. F., Slutsker, I., Abuhassan, N., Newcomb, W. W., Schafer, J., Chatenet, B., Lavenu, F., Kaufman,
Y. J., Vande Castle, J., Setzer, A., Markham, B., Clark, D., Frouin, R., Halthore, R., Karnieli, A., O’Neill, N. T., Pietras, C., Pinker, R. T.,
Voss, K., and Zibordi, G.: An emerging ground-based aerosol climatology: Aerosol Optical Depth from AERONET, *J. Geophys. Res.*,
106, 12 067–12 097, 2001.
- Knippertz, P. and Todd, M. C.: The central west Saharan dust hot spot and its relation to African easterly waves and extratropical disturbances,
385 *Journal of Geophysical Research*, 115, <https://doi.org/10.1029/2009jd012819>, 2010.
- Lavaysse, C., Chaboureau, J.-P., and Flamant, C.: Dust impact on the West African heat low in summertime, *Quarterly Journal of the Royal
Meteorological Society*, 137, 1227–1240, <https://doi.org/https://doi.org/10.1002/qj.844>, 2011.
- Marécal, V., Peuch, V.-H., Andersson, C., Andersson, S., Arteta, J., Beekmann, M., Benedictow, A., Bergström, R., Bessagnet, B., Cansado,
A., Chéroux, F., Colette, A., Coman, A., Curier, R. L., Denier van der Gon, H. A. C., Drouin, A., Elbern, H., Emili, E., Engelen, R. J.,



- 390 Eskes, H. J., Foret, G., Friese, E., Gauss, M., Giannaros, C., Guth, J., Joly, M., Jaumouillé, E., Josse, B., Kadygrov, N., Kaiser, J. W.,
Krajsek, K., Kuenen, J., Kumar, U., Liora, N., Lopez, E., Malherbe, L., Martinez, I., Melas, D., Meleux, F., Menut, L., Moinat, P.,
Morales, T., Parmentier, J., Piacentini, A., Plu, M., Poupkou, A., Queguiner, S., Robertson, L., Rouïl, L., Schaap, M., Segers, A., Sofiev,
M., Tarasson, L., Thomas, M., Timmermans, R., Valdebenito, A., van Velthoven, P., van Versendaal, R., Vira, J., and Ung, A.: A regional
air quality forecasting system over Europe: the MACC-II daily ensemble production, *Geoscientific Model Development*, 8, 2777–2813,
395 <https://doi.org/10.5194/gmd-8-2777-2015>, 2015.
- Marsham, J. H., Knippertz, P., Dixon, N. S., Parker, D. J., and Lister, G. M. S.: The importance of the representation of deep
convection for modeled dust-generating winds over West Africa during summer, *Geophysical Research Letters*, 38, n/a–n/a,
<https://doi.org/10.1029/2011gl048368>, 2011.
- Marticorena, B., Chatenet, B., Rajot, J. L., Traoré, S., Coulibaly, M., Diallo, A., Koné, I., Maman, A., NDiaye, T., and Zakou, A.: Temporal
400 variability of mineral dust concentrations over West Africa: analyses of a pluriannual monitoring from the AMMA Sahelian Dust Transect,
Atmospheric Chemistry and Physics, 10, 8899–8915, <https://doi.org/10.5194/acp-10-8899-2010>, 2010.
- Martin, A., Weissmann, M., Reitebuch, O., Rennie, M., Geiß, A., and Cress, A.: Validation of Aeolus winds using radiosonde observations
and numerical weather prediction model equivalents, *Atmospheric Measurement Techniques*, 14, 2167–2183, <https://doi.org/10.5194/amt-14-2167-2021>, 2021.
- 405 Menut, L.: Modeling of Mineral Dust Emissions with a Weibull Wind Speed Distribution Including Subgrid-Scale Orography Variance,
Journal of Atmospheric and Oceanic Technology, 35, 1221–1236, <https://doi.org/10.1175/JTECH-D-17-0173.1>, 2018.
- Menut, L., C.Schmechtig, and B.Marticorena: Sensitivity of the sandblasting fluxes calculations to the soil size distribution accuracy, *Journal*
of Atmospheric and Oceanic Technology, 22, 1875–1884, 2005.
- Menut, L., Bessagnet, B., Briant, R., Cholakian, A., Couvidat, F., Mailler, S., Pennel, R., Siour, G., Tuccella, P., Turquety, S.,
410 and Valari, M.: The CHIMERE v2020r1 online chemistry-transport model, *Geoscientific Model Development*, 14, 6781–6811,
<https://doi.org/10.5194/gmd-14-6781-2021>, 2021.
- Powers, J. G., Klemp, J. B., Skamarock, W. C., Davis, C. A., Dudhia, J., Gill, D. O., Coen, J. L., Gochis, D. J., Ahmadov, R., Peckham, S. E.,
Grell, G. A., Michalakes, J., Trahan, S., Benjamin, S. G., Alexander, C. R., Dimego, G. J., Wang, W., Schwartz, C. S., Romine, G. S., Liu,
Z., Snyder, C., Chen, F., Barlage, M. J., Yu, W., and Duda, M. G.: The Weather Research and Forecasting Model: Overview, System Efforts,
415 and Future Directions, *Bulletin of the American Meteorological Society*, 98, 1717–1737, <https://doi.org/10.1175/BAMS-D-15-00308.1>,
2017.
- Richardson, D. S.: Measures of skill and value of ensemble prediction systems, their interrelationship and the effect of ensemble size,
Quarterly Journal of the Royal Meteorological Society, 127, 2473–2489, 2001.
- Rouïl, L., Honoré, C., Vautard, R., Beekmann, M., Bessagnet, B., Malherbe, L., Meleux, F., Dufour, A., Elichegaray, C., Flaud, J., Menut, L.,
420 Martin, D., Peuch, A., Peuch, V., and Poisson, N.: PREV’AIR : an operational forecasting and mapping system for air quality in Europe,
Bull Am Meteorol Soc, 90, 73–83, <https://doi.org/10.1175/2008BAMS2390.1>, 2009.
- Toth, Z., Zhu, Y., and Marchok, T.: The Use of Ensembles to Identify Forecasts with Small and Large Uncertainty, *Weather and Forecasting*,
16, 463–477, 2001.
- Vautard, R.: Is regional air quality model diversity representative of uncertainty for ozone simulation?, *Geophysical Research Letters*, 33,
425 L24 818, <https://doi.org/10.1029/2006GL027610>, 2006.